Palaeogeography, Palaeoclimatology, Palaeoecology 663 (2025) 112798

Contents lists available at ScienceDirect

Palaeogeography, Palaeoclimatology, Palaeoecology

journal homepage: www.elsevier.com/locate/palaeo

Historical inputs and biogeochemical transformations of dissolved organic matter since 1850 CE in a small plateau-lake, Southwest China

Shuaidong Li [a], Xiaolei Wang [a], Jinliang Liu [a], Yanhui Zhang [a], Robert G.M. Spencer [b], Anne M. Kellerman [b], Amy M. McKenna [c], Xiaohua Ma [d], Quanliang Jiang [e], Tao Huang [f], Hao Yang [f], Changchun Huang [f,*]

[a] School of Environmental Science, Nanjing Xiaozhuang University, Nanjing 211171, PR China
[b] Department of Earth, Ocean and Atmospheric Science, Florida State University, Tallahassee, FL 32306, USA
[c] National High Magnetic Field Laboratory, Florida State University, Tallahassee, FL 32310, USA
[d] School of Geography, Jiangsu Second Normal University, Nanjing 210013, PR China
[e] School of environment and surveying engineering, Suzhou University, Suzhou 234000, PR China
[f] School of Geography, Nanjing Normal University, Nanjing 210023, PR China

ARTICLE INFO

Editor Name: Dr. Howard Falcon-Lang

Keywords:
Dissolved organic matter
Lake sediment
Spectrometry
FT-ICR MS
Historical transformation

ABSTRACT

Small lakes on the Yunnan-Kweichow Plateau of Southwest China are significant carbon sinks, and highly sensitive recorders of global climate change and human disturbance. However, the lack of robust sediment chronologies makes it challenging to unravel the dynamics of dissolved organic matter (DOM) accumulation in these sedimentary successions, and the driving mechanisms of change over historical timescales. In this paper, we constructed a robust chronology (1850–2019 CE) based on radioactive lead (^{210}Pb) for Xihu Lake, and used elemental analysis, optical spectroscopy, Fourier transform ion cyclotron resonance mass spectrometry (FT-ICR MS) and stable carbon isotopic measurements to evaluate long-term variations in the abundance, source and composition of sedimentary DOM. We found that DOM abundance increased after 2000 CE due to intensive socio-economic activities and climatic warming within the watershed. Stable carbon isotopic results are consistent with spectral parameters, suggesting the additional DOM abundance was mainly derived from annual input from autochthonous aquatic plants. These autochthonous sources shifted the DOM pool into saturated and S-containing aliphatic compound and protein-like fluorescence component, which had higher bio-lability and mineralization potential. After successive mineralization for hundreds of years, sedimentary DOM underwent a transition characterized by reduced bio-lability and increased persistence with time gradients. More oxygenated, aromatic and high-molecular-weight DOM fractions were preserved in deeper and older sediments, which became a key component of lake carbon sinks. Furthermore, massive diagenetic transformations resulted in an increasing tendency in diversity and richness of molecular assemblage. This work provides a comprehensive understanding of historical inputs, degradations and preservations of sedimentary DOM, and offers new insights into our understanding of DOM dynamics from a paleolimnological perspective.

1. Introduction

Inland lakes serve as crucial biogeochemical reactors in the regional and global carbon cycles (Cole et al., 2007). They receive substantial organic carbon (OC) inputs from catchment areas and aquatic photosynthesis, and emit carbon dioxide (CO_2) and methane (CH_4) into the atmosphere (Tranvik et al., 2009; Bastviken et al., 2011; Raymond et al., 2013). A fraction of OC is deposited in lake sediments, where it undergoes degradation. Inland lake sediments exhibit a higher carbon burial capacity than ocean sediments, containing 820 Pg of OC (Cole et al., 2007). However, previous studies suggest that approximately 50 % of OC in lake sediments could be stilled mineralized via microbial metabolism under anaerobic conditions (Jonsson et al., 2001; Song et al., 2021). The sequestration and release of carbon in lake sediments are critical for regulating carbon budgets and influencing climate change (Tranvik et al., 2009). With intensifying global warming and

* Corresponding author.
E-mail address: huangchangchun@njnu.edu.cn (C. Huang).

https://doi.org/10.1016/j.palaeo.2025.112798
Received 5 December 2024; Received in revised form 3 February 2025; Accepted 3 February 2025
Available online 4 February 2025

extreme weather events, the complex dynamics of sedimentary carbon pools and their driving mechanisms have attracted increasing attentions.

Dissolved organic matter (DOM) refers to a kind of heterogeneous organic mixtures, which are ubiquitous in natural environments and mediate carbon and nutrient transfer among the lithosphere, hydrosphere and atmosphere (Stubbins et al., 2010; Nebbioso and Piccolo, 2013). Lake sediments accumulate diverse aromatic and aliphatic DOM fractions from both autochthonous and allochthonous sources (Chen and Hur, 2015). In recent years, global climate changes and increasing anthropogenic activities have significantly altered sedimentary properties. Decreasing precipitation and the construction of dams and weirs have reduced the input, transport and sedimentation rate of allochthonous substances, thereby limiting recalcitrant DOM finally trapped in lake sediments (Tranvik and Jansson, 2002). Meanwhile, rapid industrialization and urbanization have increased nutrient loading and anthropogenic effluents in lakes, leading to widespread eutrophication (Toming et al., 2013; He et al., 2022). These changes have promoted the production of low-molecular-weight and labile autochthonous compounds, activating the remineralization of sedimentary DOM (Stedmon and Markager, 2005; Bai et al., 2022). Consequently, the quality and quantity of sedimentary DOM reflect the integrated outcomes of coexistent processes, including original inputs, biotic degradation and spontaneous transformation, posing challenges to understanding DOM dynamics across chronological sequences.

To reconstruct the historical dynamics of sedimentary DOM, this study employed paleolimnological approaches and multiple complementary analytical techniques. Radionuclides (^{210}Pb, ^{226}Ra and ^{137}Cs) were used to establish recent chronologies with precise dating (Sanchez-Cabeza and Ruiz-Fernández, 2012). UV–visible absorption spectroscopy and three-dimensional excitation-emission matrix fluorescence spectroscopy (EEMs), combined with parallel factor analysis (PARAFAC) modeling and established spectral parameters, have been widely applied to characterize chromophoric DOM (CDOM) and fluorescent DOM (FDOM) (Helms et al., 2008; Murphy et al., 2013). Fourier transform ion cyclotron resonance mass spectrometry (FT-ICR MS) coupled with electrospray ionization (ESI) provided high-resolution molecular characterization of DOM across different environments (Kellerman et al., 2014; Hendrickson et al., 2015). Previous reports indicated DOM molecules in lake sediments exhibit highly aromatic and unsaturated properties (H/C $<$ 1.5) and are enriched of N- or S-containing formulae due to sulfurization and biodegradation (Schmidt et al., 2011; Chen et al., 2023). Heteroatomic DOM serves as an essential nutrient source for the benthic communities, regulating the biogeochemical cycling of key elements within sediments. Recently, conceptual framework and tool of meta-metabolome ecology have been successfully applied to FT-ICR MS dataset to assess the phylogenetic α-diversity and potential transformation of molecular assemblages (Danczak et al., 2020). It provides new insights on the relationships between DOM chemistry and assembly mechanisms, and predicts spatiotemporal transformation of DOM molecules. Additionally, stable carbon isotope ratio (δ^{13}C) combined with Bayesian mixing model enables the quantification of source contributions for organic mixtures (Parnell et al., 2013).

The Yunnan-Kweichow Plateau of Southwest China hosts numerous lakes across various elevations. These lakes range in surface area from 1 km^2 to 310 km^2, with average water depths spanning from 1 m to 89.6 m, and trophic states varying from oligotrophic to highly eutrophic levels (Lu and Sun, 2023; Yang et al., 2024). While previous studies have focused on large lakes with highly ecological service and socioeconomic functions (Fu et al., 2006; Li et al., 2022), little is known about the sedimentary DOM dynamics of small lakes on the Yunnan-Kweichow Plateau. Due to their limited water volume and surface area, small lakes are more vulnerable to natural and anthropogenic disturbances. Xihu Lake, a shallow and small freshwater lake, serves as a critical drinking water source for local residents, agricultural irrigation and industrial production. The dual pressure of global climate changes and intensified human activities, which vary in temporal and spatial scales, may significantly alter the carbon budget of Xihu Lake by influencing the accumulation and degradation of sedimentary DOM. Therefore, the primary objectives of this study were to (1) elucidate the sources, distribution and composition of sedimentary DOM over the past century; (2) explore environmental, anthropogenic and biotic effects on DOM chemo-diversity; and (3) clarify the production, degradation and preservation of DOM across different sedimentary periods.

2. Material and methods

2.1. Site description and sample collection

The study site was located at Xihu Lake (100°01′ ~ 100°03′E, 26°00′ ~ 26°01′N, surface area: 3.1 km^2, maximum water depth: ~12.30 m), a freshwater plateau lake near Dali city, Yunnan province, China (Fig. 1). The lake water is primarily fed by precipitation and surface runoff, with approximately 4.33 % of its outflow discharging into Erhai Lake, the second largest freshwater lake on Yunnan-Kweichow Plateau, via the Luoshijiang River. In recent decades, rapid population growth and agricultural and tourism development have led to increased nutrient accumulation in Xihu Lake. The continuous nutrient loading of nutrient has stimulated algae growth and elevated primary productivity, ultimately resulting in eutrophication and pollution over the past two decades.

In August 2019, a sediment core (length: 68 cm, diameter: 8.4 cm)

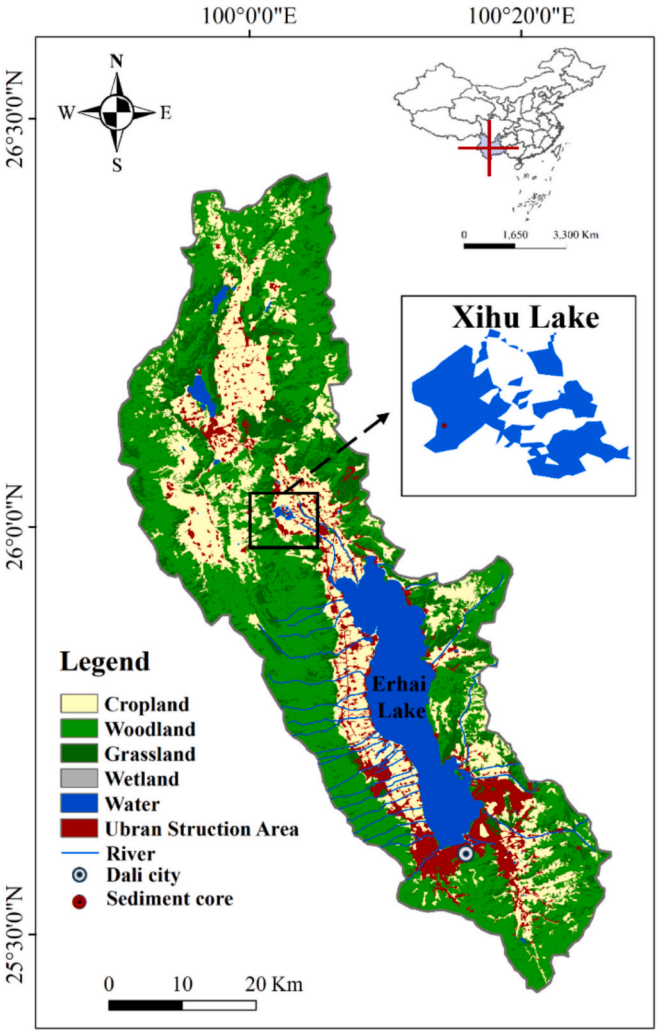

Fig. 1. Location of sampling site at Xihu Lake, China.

was collected from Xihu Lake (location: 100°02′E, 26°00′N, elevation: 1935.17 m, water depth: 5.7 m) using a gravity sediment sampler (CORER-60, Austria). The core was sliced into 1 cm thickness starting from the water-sediment interface, yielding 68 sediment samples. These samples were stored in −4 °C incubator and immediately transported to the laboratory. All samples were weighed, freeze-dried using a lyophilizer, and stored in black sealed bags for further analysis.

2.2. Laboratory analysis

2.2.1. Sediment dating

Sediment samples were stored in sealed containers for 30 days to reach secular equilibrium before radionuclides analysis. The specific activities of radionuclides (^{210}Pb, ^{226}Ra and ^{137}Cs) were measured by a high-purity Germanium (HPGe) γ-spectrometer (GWL-120-15, EG&GORTEC, USA) with a determination time of 40,000 s, and the relative detection efficiency was 62 %. The constant rate of ^{210}Pb supply (CRS) model was applied to establish the sediment core chronology (Text S1) (Sanchez-Cabeza and Ruiz-Fernández, 2012).

2.2.2. Total organic carbon (TOC), total nitrogen (TN) and grain size analyses

Total carbon (TC) and total inorganic carbon (TIC) contents were detected using a TOC analyzer (Shimadzu TOC-SSM, Japan), and TOC content was calculated as the difference between TC and TIC. TN content was measured after digestion with persulfate ($K_2S_2O_8$ + NaOH) at 121 °C by a UV-3600 spectrophotometer (Shimadzu, Japan) (Smart et al., 1983). Grain size analysis was conducted using a Malvern Mastersizer 2000 laser particle size analyzer (Malvern Instruments Ltd., UK) after organic matter and carbonate removal with 10 % hydrogen peroxide (H_2O_2) and 10 % hydrochloric acid (HCl). Sediments were classified into clay (< 4 μm), silt (4–64 μm), and sand (> 64 μm) (Folk, 1966).

2.2.3. Dissolved organic carbon (DOC), absorption and fluorescence spectroscopy analysis

Sedimentary DOM was extracted by mixing 2 g of freeze-dried sediment with ultrapure water at a 1:10 (*w/v*) ratio, shaking for 24 h at 200 rpm and 25 °C, followed by centrifugation at 5000 rpm for 15 min. Supernatants were filtered through 0.7 μm Whatman GF/ F filters (pre-burned at 450 °C for 6 h) to obtain DOM samples.

DOC concentrations were determined using a TOC analyzer (Shimadzu TOC-L, Japan) with a non-purgeable organic carbon (NPOC) assay method. The detection limit of TOC-L analyzer was 4 μg C L^{-1}, and measurements were performed with 2–3 injections, maintaining variance coefficients <2 %.

The UV–vis absorption spectroscopy was performed by a UV-3600 spectrophotometer (Shimadzu, Japan) between 200 and 800 nm at 1 nm increments, with ultrapure water as a blank. The path length of the quartz cuvette was 1 cm and absorbance precision was 0.001. Detailed information of absorbance correction and the calculation of absorption coefficient (a_λ) can be found in Text S2.

The EEMs was measured using a FS5 spectrofluorometer (Edinburgh Instruments) with excitation wavelength (Ex) from 200 to 450 nm (5 nm intervals) and emission wavelength (Em) from 250 to 600 nm (1 nm intervals). Data were corrected following standard methods (Murphy et al., 2010), and fluorescence intensities were converted to Raman units (R.U.) (Text S2). Spectral parameter such as carbon specific absorption at 254 nm ($SUVA_{254}$), spectral slope of 275 to 295 nm ($S_{275–295}$), fluorescence index (FI), biological index (BIX) and humification index (HIX) were calculated (Table S1).

2.2.4. Stable carbon isotopic analysis

DOC was firstly oxidized to CO_2 using wet-oxidation method combining persulfate and heat (Lang et al., 2012; Zhou et al., 2015). The isotopic signature of CO_2 converted from DOC was then determined by a MAT-253 isotope ratio mass spectrometer (IRMS, Thermo Fisher Scientific, Bremen, Germany) coupled with a GasBench on-line high-precision gas headspace sampler (Thermo Fisher Scientific). USGS 40 (true δ^{13}C value: - 26.39 ± 0.09 ‰, L-glutamic acid, NIST) was selected as the organic carbon standard in this study. Detailed procedures are presented in Text S3.

2.2.5. FT-ICR MS

Thirty-four sedimentary DOM samples (depth interval: 2 cm) were extracted using solid-phase extraction (SPE) for FT-ICR MS analysis (Dittmar et al., 2008). SPE-DOM samples were analyzed using a negative electrospray ionization on a 21-T FT-ICR MS at the National High Magnetic Field Laboratory in Tallahassee, Florida, USA (Hendrickson et al., 2015; Smith et al., 2018). Details of SPE process, FT-ICR MS analysis and data processing can be found in Text S4.

Molecular metrics including H/C, O/C, mass, modified aromaticity index (AI_{mod}), double-bond equivalent (DBE), and nominal oxidation state of carbon (NOSC) were calculated (Koch and Dittmar, 2006; Stubbins et al., 2010; LaRowe and Van Cappellen, 2011). Molecular compounds were classified as follows: condensed aromatics (CA), polyphenolics, highly unsaturated and phenolics with low O/C (L-HUPs), highly unsaturated and phenolics with high O/C (H-HUPs), aliphatics with low O/C (L-aliphatics), aliphatics with high O/C (H-aliphatics), peptide-like and sugar-like (Text S4). The contributions of molecular compounds and formulae were calculated by the sum of the relative abundances (%RA) of each compound and formula divided by the summed relative abundances of all assigned compounds or formulae in each sample, scaled to 10,000.

2.3. Statistical analysis

2.3.1. PARAFAC modeling

The PARAFAC modeling was conducted for all corrected EEMs dataset using DOMFluor toolbox on MATLAB R2014b (Stedmon and Bro, 2008). Residual and split-half analysis and comparisons with the OpenFlour database (http://www.openfluor. org) were applied to determine fluorescence components (Table S2) (Murphy et al., 2014). Fluorescence intensities (F_{max}) were used for component quantification.

2.3.2. Bayesian mixing model

The Bayesian mixing model combined with stable carbon isotopes were applied to calculate the source contributions for DOC by using "MixSIAR" package in R 4.2.0 software (Stock et al., 2018) (Text S5). Based on Markov chain Monte Carlo algorithm, the output of Bayesian mixing model is a probability distribution (Parnell et al., 2010; Meng et al., 2022b). This study obtained the δ^{13}C ranges of autochthonous and allochthonous endmembers from other literatures (Table S3), which were set as source tracers inputting the MixSIAR model.

2.3.3. Molecular dendrogram establishment

Following the protocols established in (Danczak et al., 2020), we established a molecular characteristics dendrogram (MCD) by computing all possible differences of molecular formulae, and a transformation-based dendrogram (TD) by assigning hypothetical molecular transformation (Text S6). A transformation-weighted characteristics dendrogram (TWCD) was subsequently generated by combing MCD and TD (Text S6), which could fuse molecular characteristics and transformation relationships. The R scripts for the establishment of MCD, TD, TWCD and transformation database are publicly available at https://github.com/danczakre/MetaMetabolome_Ecology. Finally, the TWCD was used to measure alpha-diversity indices including Faith's phylogenetic diversity (PD) and Richness by "picante" packages in R 4.2.0 software.

3. Results

3.1. Chronology and bulk characteristics of sediment

The specific activity of $^{210}Pb_{ex}$ in the sediment core ranged from 1.63 to 252.84 Bq Kg^{-1}, with an average value of 58.80 ± 51.35 Bq Kg^{-1} (mean ± standard deviation), showing an exponential decay from the surface to bottom (Fig. S1). The chronology of the sediment core was from 1850 to 2019 CE. However, no peaks in ^{137}Cs specific activity were observed in 1986, 1975 and 1963 CE (Fig. S1), suggesting that the vertical distribution of ^{137}Cs specific activity might be influenced by sediment rates, post-depositional migration and varying precipitation patterns (Ioannidou and Papastefanou, 2006; Drexler et al., 2018).

TOC and TN contents were 22.59–77.29 mg C g^{-1} and 1.23–5.98 mg N g^{-1} during 1850–2019 CE, respectively (Fig. S2). Both TOC and TN contents showed an increasing trend from the bottom to the surface of the sediment core. Silt and clay were the predominant components of the sediment (Fig. S3). The proportion of silt varied between 38.06 % and 72.75 %, with an average of 54.29 ± 7.12 %, and the proportion of clay ranged from 10.82 % to 53.85 %, with an average of 27.10 ± 12.85 %. The proportion of sand increased in the surface sediments with a drastic fluctuation, which was consistent with the median grain size (Fig. S3). These marked increases in TOC, TN contents and median grain size were associated with anthropogenic disturbances during this period.

3.2. Contents and stable carbon isotope of sedimentary DOC

DOC contents in the sediment core varied from 0.20 mg C g^{-1} to 0.88 mg C g^{-1}, exhibiting an overall increasing trend over time (Fig. 2a). Before 2000 CE, DOC contents were relatively low, with an average of 0.34 ± 0.07 mg C g^{-1}. After 2000 CE, DOC contents increased by 1.24 times (0.42 ± 0.20 mg C g^{-1}), and reach maximum in 2017 CE. The $\delta^{13}C$ values were relatively positive before 2000 CE, with a little variation (25.41 ± 0.50 ‰), but gradually decreased to an average of −28.20 ± 1.19 ‰ after 2000 CE (Fig. 2b and Fig. S4). The relative contributions of autochthonous and allochthonous endmembers for DOC were calculated using Bayesian mixing model combined with $\delta^{13}C$ values (Fig. 2c). The average $\delta^{13}C$ values for autochthonous and allochthonous endmembers from previous literatures were − 31.37 ± 2.32 ‰ and − 25.20 ± 2.34 ‰, respectively (Table S3). Allochthonous sources dominated the DOC pool, accounting for 86.94 ± 8.85 % (51.93–92.71 %), while autochthonous sources accounted for only 13.06 ± 8.85 % (7.29–48.07 %). Before 2000 CE, a steady source allocation was observed, with allochthonous sources contributing predominantly 90.62 ± 1.31 % and autochthonous sources contributing 9.38 ± 1.31 %. After 2000 CE, autochthonous sources showed a substantial increase, ranging from 12.82 % to 48.07 %.

3.3. Optical characteristics of sedimentary DOM

The optical characteristics of sedimentary DOM changed significantly during diagenesis. CDOM absorption parameters including a_{254}, $SUVA_{254}$ and $S_{275–295}$ values ranged from 55.49 to 171.50 m^{-1}, 0.82 to 1.33 L mg^{-1} m^{-1}, and 0.011 to 0.029, respectively (Fig. 3a-c). Consistent with DOC contents, similar temporal patterns were discovered in a_{254} values, which were relatively low (86.48 ± 17.02 m^{-1}) before 2000 CE and increasing by 1.10 times (94.94 ± 34.85 m^{-1}) after 2000 CE. $SUVA_{254}$ values decreased from 1.12 ± 0.07 L mg^{-1} m^{-1} to 1.02 ± 0.10 L mg^{-1} m^{-1} post-2000 CE, while $S_{275–295}$ values increased significantly (0.013–0.029) during the same phase.

The four-component PARAFAC model explained >99.9 % of the total EEMs variability, and these components were identified by comparing with online spectral library on OpenFluor database (Table S2). C1 (Ex/Em = 355/474 nm), C2 (Ex/Em = 320/394 nm) and C3 (Ex/Em = <250/440 nm) were categorized as peak C, peak M and peak A, respectively. These humic-like fluorescent peaks were associated with terrestrial origins, fulvic acids and microbial products. C4 (Ex/Em = 275/304 nm) represented protein-like fluorophores (peak T and peak B) related to autochthonous production (e.g., amino acids). The total fluorescence intensity (ΣF_{max}) increased from 3.32 to 6.92 R.U. during 1850–2019 CE, following a similar trend to DOC contents and a_{254} values (Fig. 3d). Humic-like C3 was the dominated fluorescent component, accounting for 46.11 ± 2.93 % of all fluorescent components, followed by humic-like C2 (21.47 ± 1.37 %) and C1 (20.21 ± 1.53 %) and protein-like C4 (12.22 ± 4.79 %). C4 contributed only 10.78 ± 1.25 % before 2000 CE, but increased markedly to 17.29 ± 8.09 % after 2000 CE. Fluorescent parameters including FI, BIX and HIX ranged from 1.42 to 1.69, 0.70 to 0.81, and 1.16 to 5.31, respectively (Fig. 3e-g). Both FI and BIX values gradually increased in the surface sediments, but HIX values showed a decreasing tendency.

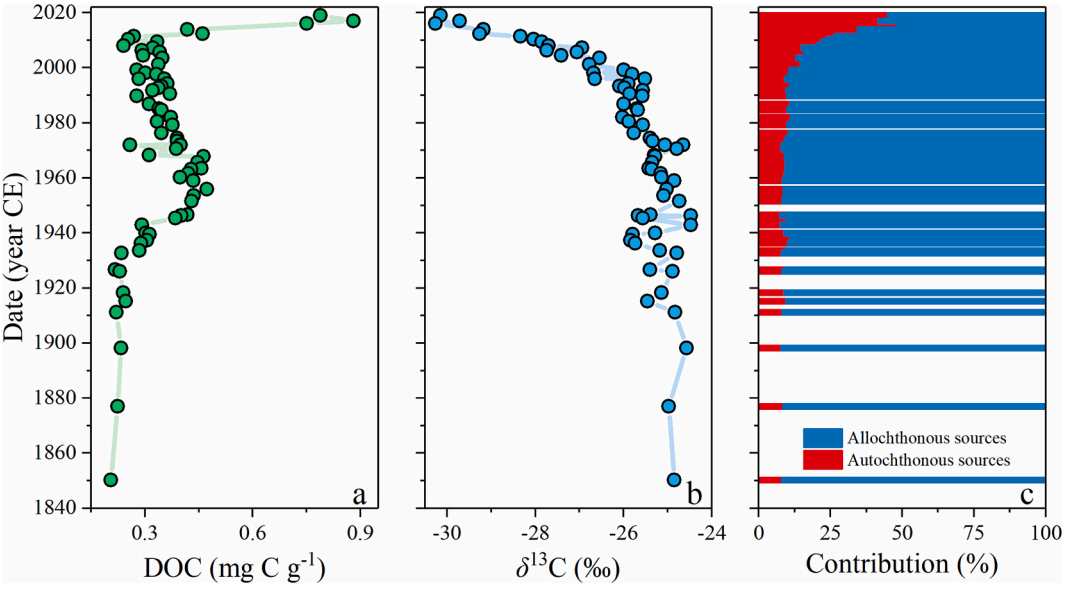

Fig. 2. Historical changes in DOC contents (a), $\delta^{13}C$ values (b) and source contributions (c) in the sediment core.

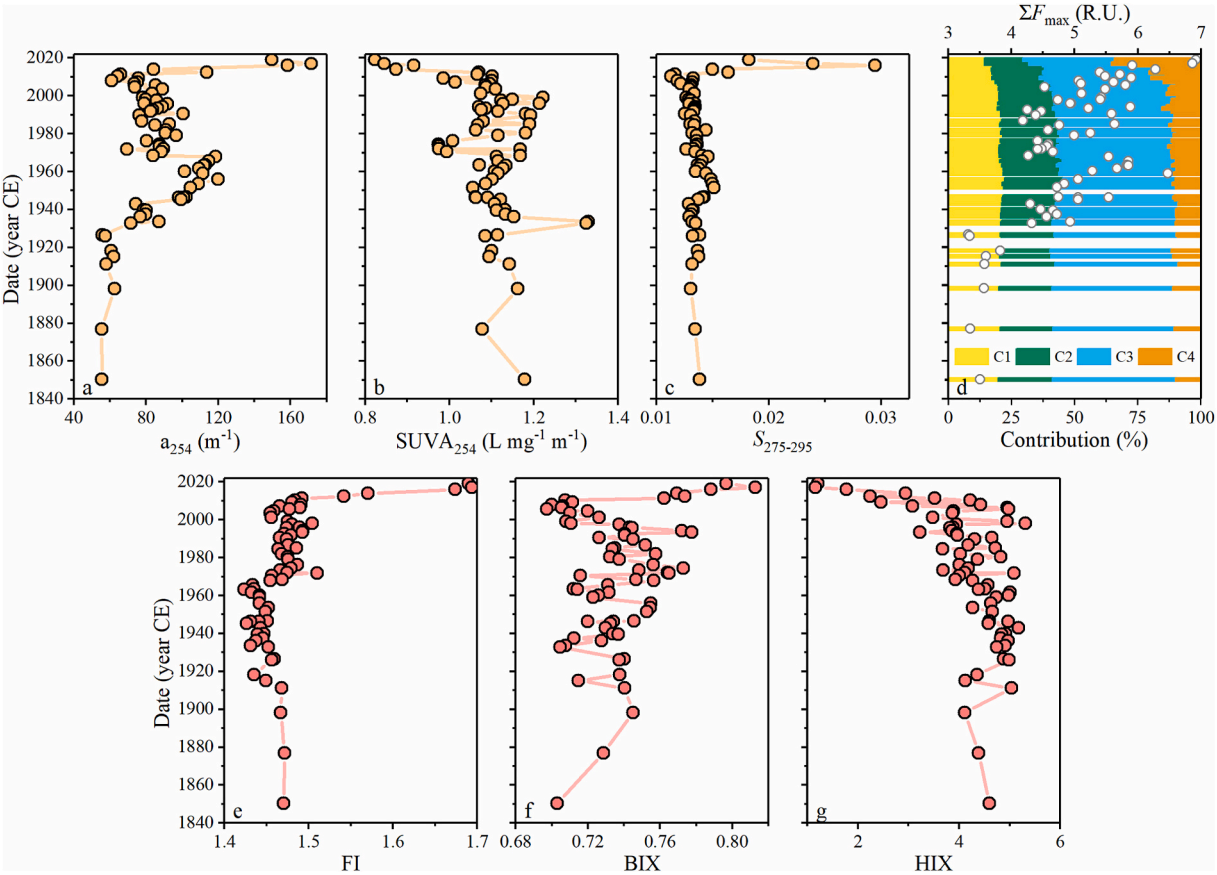

Fig. 3. Historical changes in optical characteristics of DOM in the sediment core.

3.4. Molecular complexity of sedimentary DOM by FT-ICR MS

A total of 22,575 molecular formulae were identified via FT-ICR MS from 34 sedimentary DOM samples. The number of CHO, CHOS, CHON, and CHONS formulae were 5960, 5936, 8790, and 1889, respectively (Fig. S5a). Molecular mass predominantly ranged from 180 to 945 Da, showing a normal distribution with a median of 513 Da. These formulae distributed across a wide range on the van Krevelen (V—K) plot (O/C: 0.46 ± 0.18, H/C: 1.26 ± 0.37, Fig. S5b), indicating significant molecular heterogeneity.

CHO formulae accounted for 42.38 ± 5.06 %RA, followed by CHOS (36.22 ± 7.91 %RA), CHON (18.07 ± 4.10 %RA) and CHONS (3.34 ± 0.53 %RA) formulae (Fig. S6). The relative abundance of CHO formulae increased towards the older layers, while CHOS formulae showed an inverse trend. The relative abundance of CHO formulae was higher before 2000 CE (43.36 ± 3.26 %RA) compared to that after 2000 CE (39.17 ± 7.79 %RA). In contrast, the relative abundance of CHOS formulae increased markedly to 60.44 %RA after 2000 CE. In terms of molecular compounds, HUPs compound had the highest relative abundance (H-HUPs: 21.83 ± 3.83 %RA, L-HUPs: 32.00 ± 3.73 %RA), followed by aliphatics (H-aliphatics: 11.84 ± 3.16 %RA, L-aliphatics: 20.56 ± 4.98 %RA), polyphenolics (6.50 ± 1.89 %RA), peptide-like (4.88 ± 1.07 %RA), CA (1.75 ± 0.59 %RA) and sugar-like (0.64 ± 0.27 %RA) compounds (Fig. S6). After 2000 CE, the relative abundance of aliphatics compound increased, particularly L-aliphatics compound, while the relative abundance of other compounds either decreased or remained unchanged.

To avoid the influence of different proportions of different formulae on inherently chemical characteristics, we calculated weight averaged (wa) values of all molecular metrics based on their initial values divided by the relative intensity of each formula (Fig. 4a-f). The average H/C_{wa} value was relatively higher after 2000 CE, and average values of $mass_{wa}$, O/C_{wa}, $NOSC_{wa}$, $AI_{mod\text{-}wa}$, and DBE_{wa} were relatively higher before 2000 CE. However, temporal comparisons of these molecular metrics had no statistical differences possibly due to the disturbance from common formulae ($n = 4092$) shared by all samples. A transformation-weighted characteristics dendrogram was constructed to investigate potential transformations and structural organization of molecules (Fig. S7). The number of potential transformations changed from 3 to 588, with 60–80 transformations occurring most frequently (Fig. S8a). The number of transformations was minimal in 2019 CE and became more abundant before 2000 CE (Fig. S8b). Additionally, the dendrogram-based alpha-diversity indices showed a range of 769.07 to 1066.51for PD and 8083 to 13,359 for richness (Fig. 4g-h). Both PD and richness exhibited relatively lower levels after 2000 CE, and reach minimum in 2016 CE.

4. Discussion

4.1. Variations of DOM abundance controlled by anthropogenic and environmental factors

DOM abundance (DOC, CDOM and FDOM) displayed a two-stage temporal distribution pattern, with an accelerated increasing time point around 2000 CE. The relationships between socio-economic (total population, GDP, per capita GDP and government revenue) and environmental factors (temperature, precipitation, grain size, TOC and TN) with DOC, CDOM and FDOM contents were analyzed (Fig. S9–10 and Table. S4–5). Due to the limitation in historical statistics, meteorological data from 1966 to 2019 CE and socio-economic parameters from 1952 to 2019 CE were obtained from statistical yearbook. DOM abundance was significantly positive with GDP ($r = 0.44$–0.62, $p < 0.01$), per capita GDP

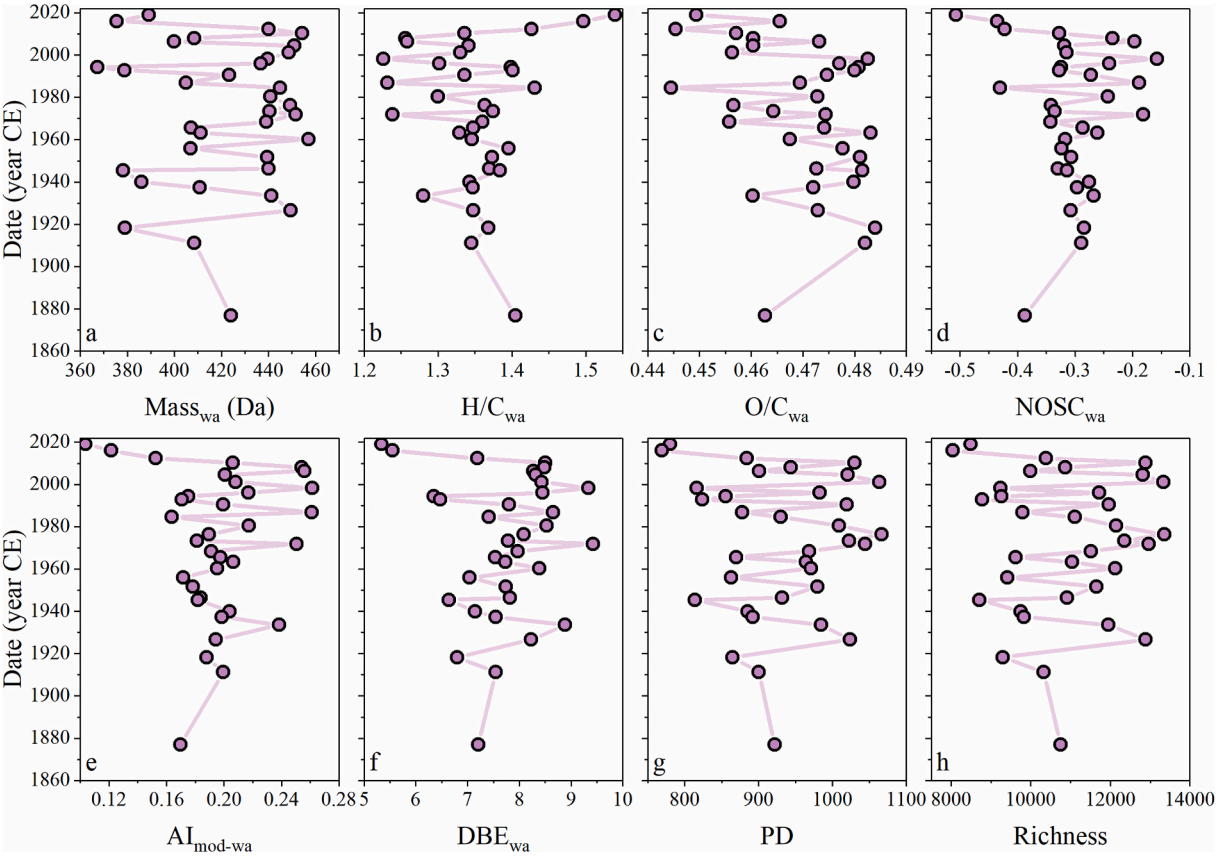

Fig. 4. Historical changes in molecular metrics (a-f) and alpha-diversity indices (g-h) of DOM in the sediment core.

($r = 0.43$–0.62, $p < 0.01$) and government revenue ($r = 0.42$–0.61, $p < 0.01$), but had no significant correlation with total population ($p > 0.05$, Table. S4). From 2000 to 2019 CE, GDP, per capita GDP and government revenue increased from 147.21 to 1374.80 × 100 million yuan, 0.44 to 3.77 × 10^4 yuan, and 21.00 to 199.27 × 100 million yuan, respectively (Fig. S9). Economic developments likely exacerbated watershed erosion and deterioration of water quality, leading to a sharp increase in sedimentary DOM in Xihu Lake (Dearing et al., 2008; Yang et al., 2022; Xiao et al., 2023). Previous study reported an earlier increase in sedimentary DOM abundance around 1980 CE in Dianchi Lake, a eutrophic lake near Kunming city (Li et al., 2022). The difference reflected the sequence of economic development and the speed of industrialization and urbanization in different regions of China. As the capital of Yunnan Province, Kunming city took the lead in entering the stage of industrialization and urbanization since the Reform and Opening Up in 1978 CE (Liu et al., 2012; Meng et al., 2022b). Consequently, DOM abundance in the surface sediments of Dianchi Lake was much higher than that of Xihu Lake.

Climate change can affect carbon inputs to aquatic systems through precipitation-induced erosion and temperature-driven hydrophyte growth (Tranvik et al., 2009). In Xihu watershed, temperature increased from 14.13 to 16.14 °C during 1966–2019 CE, showing significantly positive correlations with DOC ($r = 0.31$, $p < 0.05$) and FDOM contents ($r = 0.63$, $p < 0.001$, Table S5). This suggested that climate warming may stimulate hydrophyte growth, increasing autochthonous DOM production by elevating primary productivity (Chen et al., 2012; Zhou et al., 2018). However, DOM abundance had no significant correlation with local precipitation over the same period. Based on correlation coefficients, socio-economic factors were the most important drivers of sedimentary DOM abundance. In older layers, particularly before 1940 CE, lower DOM abundance was associated with minimal human disturbance and prolonged mineralization. The significantly positive relationship between DOM abundance and TOC contents ($r = 0.49$–0.73, $p < 0.001$, Table. S5) suggested that DOM burial is regulated by the adsorption and desorption of organic matter in sediments. Additionally, DOC, CDOM and FDOM contents had some correlations with clay and sand (Table. S5), likely influenced by changing hydrological conditions in the watershed (Hu et al., 2016; Meng et al., 2022a).

4.2. *Qualitative and quantitative apportionment of sedimentary DOM sources*

Analysis of historical DOC variations suggested that different sources contributed to DOC with distinct temporal trends due to anthropogenic activities superimposed on environmental variability. Stable carbon isotope signature was used to qualitatively identify and quantitatively apportion sedimentary DOC sources. The average values of $\delta^{13}C$ in this study were equivalent to those observed in lakes on Yunnan-Kweichow Plateau (−25.43 ± 2.94 ‰), Qinghai-Tibet Plateau (−25.77 ± 1.85 ‰) and Eastern China (−25.31 ± 2.71 ‰, Fig. S4) The depth-depended fluctuations in $\delta^{13}C$ values indicated temporal heterogeneity in source conrtibutions. Lake sediments serve as crucial carbon sinks, incorporating both terrestrial organics (soil and plant residues) and aquatic biomass produced in situ. The $\delta^{13}C$ values of terrestrial soils generally range from −29 ‰ to −23 ‰ (Derrien et al., 2018; Wen et al., 2021). Terrestrial plants, classified based on their photosynthetic pathways, exhibit distinct $\delta^{13}C$ signatures: C3 plants range from −30 ‰ to −20 ‰, C4 plants from −19 ‰ to −9 ‰, and CAM plants from −30 ‰ to −10 ‰ (Lopes et al., 2013; Xu et al., 2019). In freshwater ecosystems, phytoplankton, floating and emergent plants typically have lower $\delta^{13}C$ values than submerged plants (Xu et al., 2019). Phytoplankton, floating and emergent plants gengerally prefer to utilize atmospheric and dissolved ^{12}C-rich CO_2 ($\delta^{13}C \approx -7$ ‰) during light and photosynthesis. However, submerged plants rely on bicarbonate ($\delta^{13}C \approx 0$ ‰), increasing $\delta^{13}C$ values to −20 ‰ (Xiong et al., 2010).

The $\delta^{13}C$ characteristics of sedimentary DOC in this study was corresponded to those of terrestrial soils and C3 plants. Xihu Lake is primarily surrounded by forest and agricultural fields with high coverage of subtropical evergreen forest plants (e.g., pine, fir and spruce) and crops (e.g., paddy, wheat and tobacco). Bayesian mixing model results indicated that allochthonous organics were predominant source for sedimentary DOC pool over the past 150 years. However, agricultural fertilizers, industrial and domestic sewage led to increased nutrient loading in Xihu Lake. These coupled with climate warming have improved the primary production of aquatic plants (e.g., algae, caltrop and phragmites) over the past two decades (Williams et al., 2010; Wang and Chen, 2018). Therefore, the accumulation of decaying aquatic plant residues sustained annual increase in autochthonous contributions since 2000 CE. Compared with severely eutrophic lakes such as Taihu Lake and Dianchi Lake (Meng et al., 2021; Li et al., 2022), the proportion of autochthonous material in Xihu Lake's surface sediments remained relatively lower. Moreover, large-scale urban development, including the construction of hardened roads, has reduced surface runoff infiltration, thereby limiting the transport of allochthonous DOC into the lake (Xiao et al., 2023).

Fluorescent parameters further support these findings. The FI value can indicate FDOM sources, which has a value of >1.9 for autochthonous inputs and a value of <1.4 for allochthonous inputs (McKnight et al., 2001). The FI values ranged from 1.42 to 1.69 (1.48 ± 0.05) between 1877 and 2019 CE, indicating predominant allochthonous contribution to sedimentary FDOM. The BIX values in this study were lower (< 0.8), implying limited contributions from freshly autochthonous FDOM fractions (Huguet et al., 2009). Notably, both FI and BIX values had significantly positive correlations with autochthonous contributions calculated by Bayesian mixing model ($p < 0.001$, Fig. S11), confirming the enhanced input of aquatic plant-derived organic matter in the surface sediments. Fluorescent parameters are primarily sensitive to FDOM components and may change upon the occurrence of biogeochemical transformations (Yang and Hur, 2014; Derrien et al., 2018). Consequently, the source apportionments based on $\delta^{13}C$ values combined with Bayesian mixing model appear to better align with historical records of eutrophication in Xihu Lake.

4.3. Production, degradation and preservation of sedimentary DOM compositions over the past century

Sedimentary DOM in Xihu Lake exhibited a high abundance of heteroatomic formulae, with a significant proportion of aromatic and aliphatic compounds. Aromatic compounds were preferentially preserved under anoxic conditions, while sulfurization of organic matter and anthropogenic sewage contributed to the enrichment of S- and N-containing compounds in sediments (Chen and Hur, 2015). Due to significant variations in DOM sources over time, more heterogeneous compositions and structural characteristics of DOM were observed along the sediment core. The high abundance of humic-like fluorescent components (C1, C2 and C3) and aromatic molecular compounds such as HUPs, polyphenolics and CA compounds highlighted the dominant contribution of allochthonous DOM. The abundance of these allochthonous DOM fractions decreased after 2000 CE, while the protein-like C4 component and aliphatic compound increased due to enhanced autochthonous contribution driven by human activities (Williams et al., 2016; Liu et al., 2020). Spearman's correlation analysis ($r > 0.30$, $p < 0.05$) between the percentages of four PARAFAC components and the relative abundances of molecular formulae enabled to assign the location of each PARAFAC component in V—K plot (Fig. 5). Protein-like C4 component exhibited higher H/C ratios (1.60 ± 0.21) and lower O/C ratios (0.40 ± 0.13), which was close to low-oxidized and highly saturated L-aliphatics compounds (Fig. 5b). Humic-like components (C1, C2 and C3) clustered with HUPs and polyphenolics compounds, characterized by higher molecular weight, greater aromaticity, increased unsaturation and humification (Fig. 5b). This study demonstrated the consistency between optical technique and FT-ICR MS in DOM characterization, providing a comprehensive perspective on DOM compositions.

The pronounced stratification of DOM characteristics along the sediment core implied the distinct DOM cycling processes occurring during different historical periods. To minimize the influence of common formulae on molecular traits, we screened out the predominant formulae after 2000 CE and before 2000 CE by comparing their average relative abundance of each mass peak. The post-2000 CE samples contained a greater number of predominant molecular formulae ($n = 1157$) compared to pre-2000 CE samples ($n = 938$). These predominant formulae had distinct spatial division in V—K plots and significantly different molecular structures (Fig. S12–13). Moreover, predominant formulae after 2000 CE was mostly consisted of CHO formulae with L-aliphatics and L-HUPs compounds. Predonimant formulae before 2000 CE had a higher relative abundance of CHO, CHON and CHOS formulae with H-HUPs, H-aliphatics and peptide-like compounds (Table. S6).

Principal component analysis (PCA) effectively separated the samples, illustrating temporal variability (Fig. 6). PC1 negative loading corresponded to predominant formulae (CHOS%RA) and compounds (L-aliphatics%RA and L-HUPs%RA) after 2000 CE, along with sediment date, TN, DOC, a_{254}, ΣF_{max}, $S_{275-295}$, BIX, C4% and H/C_{wa} (Fig. 6a). All post-2000 CE samples displayed PC1 negative scores (Fig. 6b), indicating that the surface sediments had high DOM abundance and was enrich in saturated and aliphatic S-containing molecules and freshly biolabie FDOM components. Human activities and enhanced primary productivity increased anthropogenic and autochthonous organics to lake, and influenced sedimentary DOM chemistry (D'Andrilli et al., 2015;

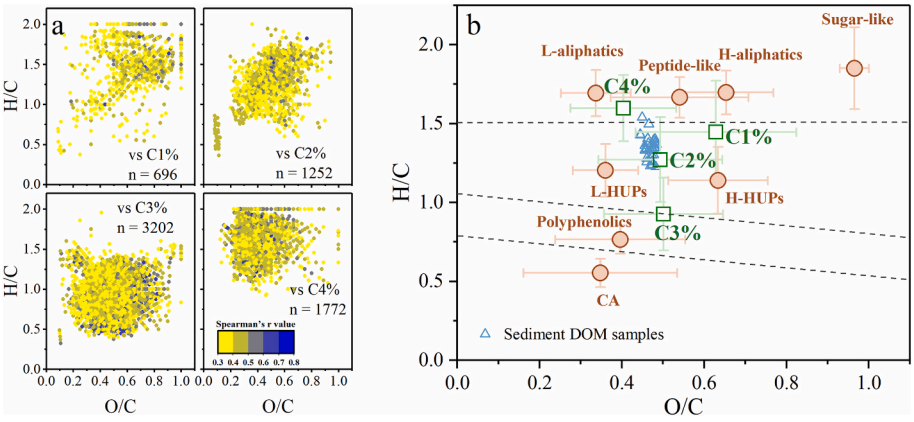

Fig. 5. Spearman's correlations between molecular formulae and PARAFAC components (a), and V—K plots showing comparison of molecular compounds and PARAFAC components based on Spearman's correlation analysis (b).

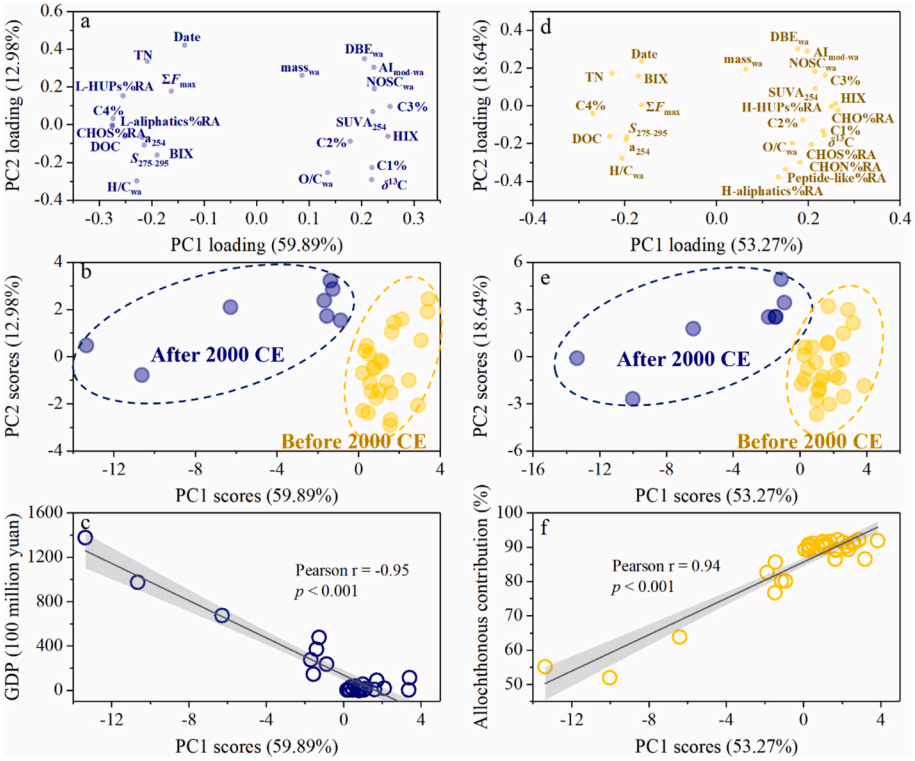

Fig. 6. PCA loading and scores of sediment date, TN, DOC, $\delta^{13}C$, spectral parameters, PARAFAC components, molecular metrics and major compositions of predominant formulae after 2000 CE (a-b), and the relationships between PC1 scores and GDP (c). PCA loading and scores of sediment date, TN, DOC, $\delta^{13}C$, spectral parameters, PARAFAC components, molecular metrics and major compositions of predominant formulae before 2000 CE (d-e), and the relationships between PC1 scores and allochthonous contribution based on Bayesian mixing model (f).

Shang et al., 2022). It could be supported by the significantly relationships between PC1 scores and GDP (Fig. 6c). These bio-labile DOM with C—S bonds were prone to demethylation, generating numerous CH_4 emissions from benthic sediments (Bizic, 2021). Previous studies found that synthetic surfactant compounds containing O_3S and O_5S, widely used for detergents in China, exhibited high abundance in urban river and wastewater (Gonsior et al., 2011; He et al., 2019). The enrichment of O_3S and O_5S compounds in the surface sediments of Xihu Lake also supported the intensive anthropogenic signal (Fig. S13h).

PC1 positive loadings corresponded to predominant formulae (CHO %RA, CHON%RA and CHOS%RA) and compounds (H-HUPs%RA, H-aliphatics%RA and peptide-like%RA) before 2000 CE, as well as humic-like FDOM components (C1%, C2% and C3%), $mass_{wa}$, DEB_{wa}, AI_{mod-wa}, $NOSC_{wa}$, O/C_{wa}, $SUVA_{254}$, HIX and $\delta^{13}C$ (Fig. 6d). All pre-2000 CE samples showed PC1 positive scores (Fig. 6e). Due to successive mineralization for hundreds of years or longer, the protein-like and aliphatic compounds were preferentially degraded, leaving the older sediments enriched in oxygenated, aromatic and high-molecular-weight compounds from allochthonous sources (Fig. 6f). The "island of stability" (IOS) with a specific range of formulae (mass: 360 ± 28 and 497 ± 51 Da, O/C: 0.52 ± 0.10, H/C: 1.17 ± 0.13) was considered to be a subset of highly persistent molecules (Lechtenfeld et al., 2014; Kellerman et al., 2018). The increased abundance of IOS in deeper sediments suggested that older sedimentary DOM underwent a transition characterized by reduced bio-lability and enhanced persistence (Fig. S13g). Although older sedimentary DOM exhibited overall stability, a slight upward trend in some active peptide-like and H-HUP compounds was observed. These compounds probably originated from slowly microbial reworking of older DOM, and were preserved under anoxic conditions in deeper sediments (Jessen et al., 2017; Chen et al., 2023). In addition, the presence of CHOS formulae was likely resulted from the early diagenetic sulfurization of CHO formulae via abiotic pathways (Schmidt et al., 2009; Melendez-Perez et al., 2016).

Interestingly, dendrogram-based alpha-diversity indices and potential transformation co-varied with intrinsic traits of DOM molecules. Previous studies reported that microbial metabolism could act as a selection pressure, influencing the structural organization of molecular assemblages (Hu et al., 2022; Li et al., 2023). In younger sediments, freshly low-molecular-weight compounds could be rapidly mineralized or transformed by starved microbial taxa, leading to decreased diversity and richness of molecular dendrogram. During early diagenesis process, the accumulation of recalcitrant high-molecular-weight and microbe-derived compounds might maintain relatively higher diversity and richness levels. This hypothesis was supported by significantly positive correlations between $mass_{wa}$ and PD ($r = 0.78$, $p < 0.001$, Fig. 7a) and richness($r = 0.86$, $p < 0.001$, Fig. 7b). The evidence that molecular assemblage was theoretically subject to microbial processing in sediments also was reflected by pattern of potential transformations over hundred years. The weight averaged number of potential transformation was significantly negative with H/C_{wa} ($r = -0.88$, $p < 0.001$, Fig. 7c) and significantly positive with AI_{mod-wa} ($r = 0.90$, $p < 0.001$, Fig. 7d), indicating saturated molecules had less potential transformations and aromatic molecules had more potential transformations. DOM molecules after biological transformations and spontaneous chemical reactions tended to become more stable, contributing to long-time carbon storage in sediments.

5. Conclusion

This study comprehensively examined the abundance, sources, intrinsic properties and influencing mechanisms of sedimentary DOM over the past century. After 2000 CE, the DOM pool in the surface sediments exhibited higher contribution of autochthonous sources, characterized by an increasing abundance of freshly protein-like and aliphatic compounds that are more biolabile, saturated, and less aromatic. These pronounced shifts in DOM chemistry were primarily driven

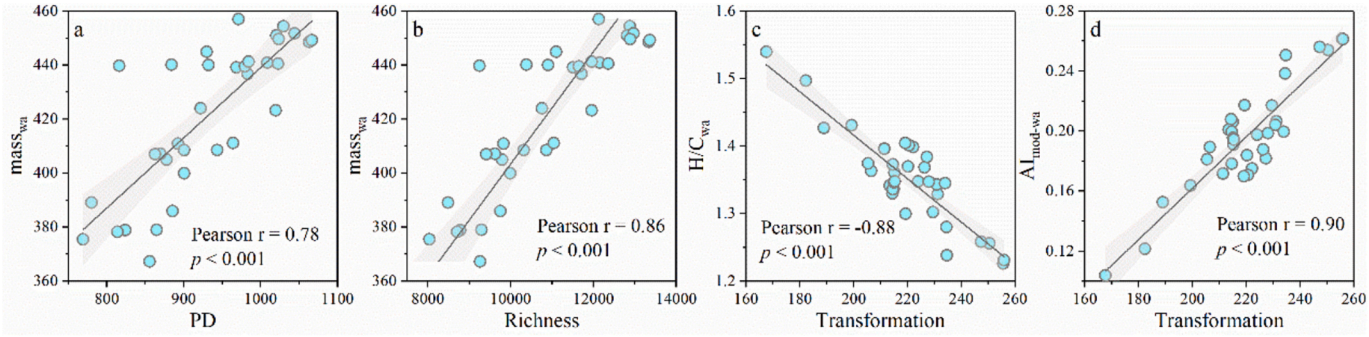

Fig. 7. The relationships between $mass_{wa}$ and PD (a) and Richness (b), and the relationships between H/C_{wa} (c) and $AI_{mod\text{-}wa}$ (d) and transformation.

by intensified anthropogenic activities and enhanced primary productivity under rapid socio-economic development and climatic warming. Over timescales of hundreds of years or longer, continuous mineralization led to the microbial degradation of bioavailable DOM fractions, resulting in the preferential preservation of high-molecular-weight and aromatic organic matter, such as humic-like component and HUPs compound, in deeper and older sediments. Moreover, the structural organization and potential transformation of molecular assemblages were closely aligned with intrinsic properties of DOM molecules. The observed decline in molecular diversity and richness was attributed to the degradation of low-molecular-weight compounds or their transformation into high-molecular-weight compounds. These transformed molecules became increasingly recalcitrant, contributing significantly to sediment carbon storage. Future research should focus on identifying source-specific markers for sedimentary DOM, and quantifying the interactions between microbial communities and DOM molecules of varying sizes and compositions. It will improve our understandings of the biochemical processes governing sedimentary DOM and their implications for regional and global carbon cycling.

CRediT authorship contribution statement

Shuaidong Li: Writing – original draft, Visualization, Software, Funding acquisition, Data curation, Conceptualization. **Xiaolei Wang:** Methodology. **Jinliang Liu:** Software, Investigation. **Yanhui Zhang:** Formal analysis. **Robert G.M. Spencer:** Writing – review & editing, Software, Resources. **Anne M. Kellerman:** Software, Data curation. **Amy M. McKenna:** Data curation. **Xiaohua Ma:** Investigation. **Quanliang Jiang:** Investigation. **Tao Huang:** Writing – review & editing, Supervision, Project administration. **Hao Yang:** Validation, Project administration. **Changchun Huang:** Writing – review & editing, Supervision, Project administration, Conceptualization.

Declaration of competing interest

We declare that we do not have any commercial or associative interest that represents a conflict of interest in connection with the submitted work.

Acknowledgements

This study was financially supported by the National Natural Science Foundation of China [U24A20577, 42277214, 42207514 and 42307325], the Natural Science Foundation of Jiangsu Province [BK20240270], the Science Foundation of the Jiangsu Higher Education Institutions of China [24KJB170012], the Key Project of Natural Science of Anhui Provincial Department of Education, China [2023AH052231], the Quality Engineering Project of Anhui Provincial Department of Education [2023zybj043] and the Talent Introduction Project of Nanjing Xiaozhuang University. The Ion Cyclotron Resonance user facility at the National High Magnetic Field Laboratory at Florida State University is supported by the National Science Foundation Division of Materials Research and Division of Chemistry through DMR 16-44779, and the State of Florida.

Appendix A. Supplementary data

Supplementary data to this article can be found online at https://doi.org/10.1016/j.palaeo.2025.112798.

Data availability

Data will be made available on request.

References

Bai, L., Liu, X., Hua, K., Deng, J., Wang, C., Jiang, H., Wang, A., 2022. Seasonal variations of fluorescent dissolved organic matter control estrone biodegradation potential in eutrophic waters affected by allochthonous and autochthonous sources. J. Hydrol. 612, 128227.
Bastviken, D., Tranvik, L.J., Downing, J.A., Crill, P.M., Enrich-Prast, A., 2011. Freshwater methane emissions offset the continental carbon sink. Science 331 (6013), 50.
Bizic, M., 2021. Phytoplankton photosynthesis: an unexplored source of biogenic methane emission from oxic environments. J. Plankton Res. 43 (6), 822–830.
Chen, M., Hur, J., 2015. Pre-treatments, characteristics, and biogeochemical dynamics of dissolved organic matter in sediments: a review. Water Res. 79, 10–25.
Chen, X., Chuai, X., Yang, L., Zhao, H., 2012. Climatic warming and overgrazing induced the high concentration of organic matter in Lake Hulun, a large shallow eutrophic steppe lake in northern China. Sci. Total Environ. 431, 332–338.
Chen, X., Cai, R., Zhuo, X., Chen, Q., He, C., Sun, J., Zhang, Y., Zheng, Q., Shi, Q., Jiao, N., 2023. Niche differentiation of microbial community shapes vertical distribution of recalcitrant dissolved organic matter in deep-sea sediments. Environ. Int. 178, 108080.
Cole, J.J., Prairie, Y.T., Caraco, N.F., McDowell, W.H., Tranvik, L.J., Striegl, R.G., Duarte, C.M., Kortelainen, P., Downing, J.A., Middelburg, J.J., 2007. Plumbing the global carbon cycle: integrating inland waters into the terrestrial carbon budget. Ecosystems 10, 172–185.
Danczak, R.E., Chu, R.K., Fansler, S.J., Goldman, A.E., Graham, E.B., Tfaily, M.M., Toyoda, J., Stegen, J.C., 2020. Using metacommunity ecology to understand environmental metabolomes. Nat. Commun. 11 (1), 6369.
D'Andrilli, J., Cooper, W.T., Foreman, C.M., Marshall, A.G., 2015. An ultrahigh-resolution mass spectrometry index to estimate natural organic matter lability. Rapid Commun. Mass Spectrom. 29 (24), 2385–2401.
Dearing, J.A., Jones, R., Shen, J., Yang, X., Boyle, J., Foster, G., Crook, D., Elvin, M., 2008. Using multiple archives to understand past and present climate–human–environment interactions: the lake Erhai catchment, Yunnan Province, China. J. Paleolimnol. 40, 3–31.
Derrien, M., Kim, M.-S., Ock, G., Hong, S., Cho, J., Shin, K.-H., Hur, J., 2018. Estimation of different source contributions to sediment organic matter in an agricultural-forested watershed using end member mixing analyses based on stable isotope ratios and fluorescence spectroscopy. Sci. Total Environ. 618, 569–578.
Dittmar, T., Koch, B., Hertkorn, N., Kattner, G., 2008. A simple and efficient method for the solid-phase extraction of dissolved organic matter (SPE-DOM) from seawater. Limnol. Oceanogr. 6 (6), 230–235.
Drexler, J.Z., Fuller, C.C., Archfield, S., 2018. The approaching obsolescence of 137Cs dating of wetland soils in North America. Quat. Sci. Rev. 199, 83–96.
Folk, R.L., 1966. A review of grain-size parameters. Sedimentology 6 (2), 73–93.
Fu, P., Wu, F., Liu, C.-Q., Wei, Z., Bai, Y., Liao, H., 2006. Spectroscopic characterization and molecular weight distribution of dissolved organic matter in sediment porewaters from Lake Erhai, Southwest China. Biogeochemistry 81, 179–189.
Gonsior, M., Zwartjes, M., Cooper, W.J., Song, W., Ishida, K.P., Tseng, L.Y., Jeung, M.K., Rosso, D., Hertkorn, N., Schmitt-Kopplin, P., 2011. Molecular characterization of

effluent organic matter identified by ultrahigh resolution mass spectrometry. Water Res. 45 (9), 2943–2953.
He, D., He, C., Li, P., Zhang, X., Shi, Q., Sun, Y., 2019. Optical and molecular signatures of dissolved organic matter reflect anthropogenic influence in a coastal river, Northeast China. J. Environ. Qual. 48 (3), 603–613.
He, D., Li, P., He, C., Wang, Y., Shi, Q., 2022. Eutrophication and watershed characteristics shape changes in dissolved organic matter chemistry along two river-estuarine transects. Water Res. 214, 118196.
Helms, J.R., Stubbins, A., Ritchie, J.D., Minor, E.C., Kieber, D.J., Mopper, K., 2008. Absorption spectral slopes and slope ratios as indicators of molecular weight, source, and photobleaching of chromophoric dissolved organic matter. Limnol. Oceanogr. 53 (3), 955–969.
Hendrickson, C.L., Quinn, J.P., Kaiser, N.K., Smith, D.F., Blakney, G.T., Chen, T., Marshall, A.G., Weisbrod, C.R., Beu, S.C., 2015. 21 Tesla Fourier transform ion cyclotron resonance mass spectrometer: a national resource for ultrahigh resolution mass analysis. J. Am. Soc. Mass Spectrom. 26 (9), 1626–1632.
Hu, L., Shi, X., Bai, Y., Qiao, S., Li, L., Yu, Y., Yang, G., Ma, D., Guo, Z., 2016. Recent organic carbon sequestration in the shelf sediments of the Bohai Sea and Yellow Sea, China. J. Mar. Syst. 155, 50–58.
Hu, A., Choi, M., Tanentzap, A.J., Liu, J., Jang, K.-S., Lennon, J.T., Liu, Y., Soininen, J., Lu, X., Zhang, Y., 2022. Ecological networks of dissolved organic matter and microorganisms under global change. Nat. Commun. 13 (1), 3600.
Huguet, A., Vacher, L., Relexans, S., Saubusse, S., Froidefond, J.-M., Parlanti, E., 2009. Properties of fluorescent dissolved organic matter in the Gironde Estuary. Org. Geochem. 40 (6), 706–719.
Ioannidou, A., Papastefanou, C., 2006. Precipitation scavenging of 7Be and 137Cs radionuclides in air. J. Environ. Radioact. 85 (1), 121–136.
Jessen, G.L., Lichtschlag, A., Ramette, A., Pantoja, S., Rossel, P.E., Schubert, C.J., Struck, U., Boetius, A., 2017. Hypoxia causes preservation of labile organic matter and changes seafloor microbial community composition (Black Sea). Sci. Adv. 3 (2), e1601897.
Jonsson, A., Meili, M., Bergström, A.-K., Jansson, M., 2001. Whole-lake mineralization of allochthonous and autochthonous organic carbon in a large humic lake (Örträsket, N. Sweden). Limnol. Oceanogr. 46 (7), 1691–1700.
Kellerman, A.M., Dittmar, T., Kothawala, D.N., Tranvik, L.J., 2014. Chemodiversity of dissolved organic matter in lakes driven by climate and hydrology. Nat. Commun. 5 (1), 3804.
Kellerman, A.M., Guillemette, F., Podgorski, D.C., Aiken, G.R., Butler, K.D., Spencer, R. G., 2018. Unifying concepts linking dissolved organic matter composition to persistence in aquatic ecosystems. Environ. Sci. Technol. 52 (5), 2538–2548.
Koch, B.P., Dittmar, T., 2006. From mass to structure: an aromaticity index for high-resolution mass data of natural organic matter. Rapid Commun. Mass Spectrom. 20 (5), 926–932.
Lang, S.Q., Bernasconi, S.M., Früh-Green, G.L., 2012. Stable isotope analysis of organic carbon in small (μg C) samples and dissolved organic matter using a GasBench preparation device. Rapid Commun. Mass Spectrom. 26 (1), 9–16.
LaRowe, D.E., Van Cappellen, P., 2011. Degradation of natural organic matter: a thermodynamic analysis. Geochim. Cosmochim. Acta 75 (8), 2030–2042.
Lechtenfeld, O.J., Kattner, G., Flerus, R., McCallister, S.L., Schmitt-Kopplin, P., Koch, B. P., 2014. Molecular transformation and degradation of refractory dissolved organic matter in the Atlantic and Southern Ocean. Geochim. Cosmochim. Acta 126, 321–337.
Li, S., Fang, J., Zhu, X., Spencer, R.G., Álvarez-Salgado, X.A., Deng, Y., Huang, T., Yang, H., Huang, C., 2022. Properties of sediment dissolved organic matter respond to eutrophication and interact with bacterial communities in a plateau lake. Environ. Pollut. 301, 118996.
Li, P., Wu, M., Li, T., Dumbrell, A.J., Saleem, M., Kuang, L., Luan, L., Wang, S., Li, Z., Jiang, J., 2023. Molecular weight of dissolved organic matter determines its interactions with microbes and its assembly processes in soils. Soil Biol. Biochem. 184, 109117.
Liu, L.-Y., Wang, J.-Z., Wei, G.-L., Guan, Y.-F., Wong, C.S., Zeng, E.Y., 2012. Sediment records of polycyclic aromatic hydrocarbons (PAHs) in the continental shelf of China: implications for evolving anthropogenic impacts. Environ. Sci. Technol. 46 (12), 6497–6504.
Liu, D., Du, Y., Yu, S., Luo, J., Duan, H., 2020. Human activities determine quantity and composition of dissolved organic matter in lakes along the Yangtze River. Water Res. 168, 115132.
Lopes, R.P., Ribeiro, A.M., Dillenburg, S.R., Schultz, C.L., 2013. Late middle to late Pleistocene paleoecology and paleoenvironments in the coastal plain of Rio Grande do Sul State, Southern Brazil, from stable isotopes in fossils of Toxodon and Stegomastodon. Palaeogeogr. Palaeoclimatol. Palaeoecol. 369, 385–394.
Lu, L., Sun, H., 2023. Dynamic monitoring of surface water areas of nine plateau lakes in Yunnan Province using long time-series Landsat imagery based on the Google Earth Engine platform. Geocarto Int. 38 (1), 2253196.
McKnight, D.M., Boyer, E.W., Westerhoff, P.K., Doran, P.T., Kulbe, T., Andersen, D.T., 2001. Spectrofluorometric characterization of dissolved organic matter for indication of precursor organic material and aromaticity. Limnol. Oceanogr. 46 (1), 38–48.
Melendez-Perez, J.J., Martínez-Mejía, M.J., Awan, A.T., Fadini, P.S., Mozeto, A.A., Eberlin, M.N., 2016. Characterization and comparison of riverine, lacustrine, marine and estuarine dissolved organic matter by ultra-high resolution and accuracy Fourier transform mass spectrometry. Org. Geochem. 101, 99–107.
Meng, L., Zhao, Z., Lu, L., Zhou, J., Luo, D., Fan, R., Li, S., Jiang, Q., Huang, T., Yang, H., 2021. Source identification of particulate organic carbon using stable isotopes and n-alkanes: modeling and application. Water Res. 197, 117083.
Meng, L., Yu, H., Bai, Y., Shang, N., Shi, K., Ji, M., Chen, R., Huang, T., Yang, H., Huang, C., 2022a. Nonhomologous black carbon decoupled char and soot sequestration based on stable carbon isotopes in Tibetan plateau lake sediment. Environ. Sci. Technol. 56 (24), 18069–18078.
Meng, L., Yue, S., Yu, H., Huang, T., Huang, C., Yang, H., 2022b. Coal combustion facilitating faster burial of char than soot in a plateau lake of Southwest China. J. Hazard. Mater. 436, 129209.
Murphy, K.R., Butler, K.D., Spencer, R.G., Stedmon, C.A., Boehme, J.R., Aiken, G.R., 2010. Measurement of dissolved organic matter fluorescence in aquatic environments: an interlaboratory comparison. Environ. Sci. Technol. 44 (24), 9405–9412.
Murphy, K.R., Stedmon, C.A., Graeber, D., Bro, R., 2013. Fluorescence spectroscopy and multi-way techniques. PARAFAC. Anal. Methods 5 (23), 6557–6566.
Murphy, K., Stedmon, C., Wenig, P., Bro, R., 2014. OpenFluor-an online spectral library of auto-fluorescence by organic compounds in the environment. Anal. Methods 6, 658–661.
Nebbioso, A., Piccolo, A., 2013. Molecular characterization of dissolved organic matter (DOM): a critical review. Anal. Bioanal. Chem. 405, 109–124.
Parnell, A.C., Inger, R., Bearhop, S., Jackson, A.L., 2010. Source partitioning using stable isotopes: coping with too much variation. PLoS ONE 5 (3), e9672.
Parnell, A.C., Phillips, D.L., Bearhop, S., Semmens, B.X., Ward, E.J., Moore, J.W., Jackson, A.L., Grey, J., Kelly, D.J., Inger, R., 2013. Bayesian stable isotope mixing models. Environmetrics 24 (6), 387–399.
Raymond, P.A., Hartmann, J., Lauerwald, R., Sobek, S., McDonald, C., Hoover, M., Butman, D., Striegl, R., Mayorga, E., Humborg, C., 2013. Global carbon dioxide emissions from inland waters. Nature 503 (7476), 355–359.
Sanchez-Cabeza, J., Ruiz-Fernández, A., 2012. ^{210}Pb sediment radiochronology: an integrated formulation and classification of dating models. Geochim. Cosmochim. Acta 82, 183–200.
Schmidt, F., Elvert, M., Koch, B.P., Witt, M., Hinrichs, K.-U., 2009. Molecular characterization of dissolved organic matter in pore water of continental shelf sediments. Geochim. Cosmochim. Acta 73 (11), 3337–3358.
Schmidt, F., Koch, B.P., Elvert, M., Schmidt, G., Witt, M., Hinrichs, K.-U., 2011. Diagenetic transformation of dissolved organic nitrogen compounds under contrasting sedimentary redox conditions in the Black Sea. Environ. Sci. Technol. 45 (12), 5223–5229.
Shang, Y., Wen, Z., Song, K., Liu, G., Lai, F., Lyu, L., Li, S., Tao, H., Hou, J., Fang, C., 2022. Natural versus anthropogenic controls on the dissolved organic matter chemistry in lakes across China: Insights from optical and molecular level analyses. Water Res. 221, 118779.
Smart, M.M., Rada, R.G., Donnermeyer, G.N., 1983. Determination of total nitrogen in sediments and plants using persulfate digestion. An evaluation and comparison with the Kjeldahl procedure. Water Res. 17 (9), 1207–1211.
Smith, D.F., Podgorski, D.C., Rodgers, R.P., Blakney, G.T., Hendrickson, C.L., 2018. 21 tesla FT-ICR mass spectrometer for ultrahigh-resolution analysis of complex organic mixtures. Anal. Chem. 90 (3), 2041–2047.
Song, X., Zhang, C., Su, X., Zhu, L., Wei, Z., Zhao, Y., 2021. Characteristics of humic substance in lake sediments: the case of lakes in northeastern China. J. Hydrol. 603, 127079.
Stedmon, C.A., Bro, R., 2008. Characterizing dissolved organic matter fluorescence with parallel factor analysis: a tutorial. Limnol. Oceanogr. Methods 6 (11), 572–579.
Stedmon, C.A., Markager, S., 2005. Tracing the production and degradation of autochthonous fractions of dissolved organic matter by fluorescence analysis. Limnol. Oceanogr. 50 (5), 1415–1426.
Stock, B.C., Jackson, A.L., Ward, E.J., Parnell, A.C., Phillips, D.L., Semmens, B.X., 2018. Analyzing mixing systems using a new generation of Bayesian tracer mixing models. PeerJ 6, e5096.
Stubbins, A., Spencer, R.G., Chen, H., Hatcher, P.G., Mopper, K., Hernes, P.J., Mwamba, V.L., Mangangu, A.M., Wabakanghanzi, J.N., Six, J., 2010. Illuminated darkness: Molecular signatures of Congo River dissolved organic matter and its photochemical alteration as revealed by ultrahigh precision mass spectrometry. Limnol. Oceanogr. 55 (4), 1467–1477.
Toming, K., Tuvikene, L., Vilbaste, S., Agasild, H., Viik, M., Kisand, A., Feldmann, T., Martma, T., Jones, R.I., Nõges, T., 2013. Contributions of autochthonous and allochthonous sources to dissolved organic matter in a large, shallow, eutrophic lake with a highly calcareous catchment. Limnol. Oceanogr. 58 (4), 1259–1270.
Tranvik, L.J., Jansson, M., 2002. Terrestrial export of organic carbon. Nature 415 (6874), 861–862.
Tranvik, L.J., Downing, J.A., Cotner, J.B., Loiselle, S.A., Striegl, R.G., Ballatore, T.J., Dillon, P., Finlay, K., Fortino, K., Knoll, L.B., 2009. Lakes and reservoirs as regulators of carbon cycling and climate. Limnol. Oceanogr. 54 (6part2), 2298–2314.
Wang, M., Chen, Y., 2018. Generation and characterization of DOM in wastewater treatment processes. Chemosphere 201, 96–109.
Wen, Z., Shang, Y., Lyu, L., Liu, G., Hou, J., He, C., Shi, Q., He, D., Song, K., 2021. Sources and composition of riverine dissolved organic matter to marginal seas from mainland China. J. Hydrol. 603, 127152.
Williams, C.J., Yamashita, Y., Wilson, H.F., Jaffé, R., Xenopoulos, M.A., 2010. Unraveling the role of land use and microbial activity in shaping dissolved organic matter characteristics in stream ecosystems. Limnol. Oceanogr. 55 (3), 1159–1171.
Williams, C.J., Frost, P.C., Morales-Williams, A.M., Larson, J.H., Richardson, W.B., Chiandet, A.S., Xenopoulos, M.A., 2016. Human activities cause distinct dissolved organic matter composition across freshwater ecosystems. Glob. Chang. Biol. 22 (2), 613–626.
Xiao, T., Ran, F., Li, Z., Wang, S., Nie, X., Liu, Y., Yang, C., Tan, M., Feng, S., 2023. Sediment organic carbon dynamics response to land use change in diverse watershed anthropogenic activities. Environ. Int. 172, 107788.

Xiong, Y., Wu, F., Fang, J., Wang, L., Li, Y., Liao, H., 2010. Organic geochemical record of environmental changes in Lake Dianchi, China. J. Paleolimnol. 44, 217–231.
Xu, J., Lyu, H., Xu, X., Li, Y., Li, Z., Lei, S., Bi, S., Mu, M., Du, C., Zeng, S., 2019. Dual stable isotope tracing the source and composition of POM during algae blooms in a large and shallow eutrophic lake: all contributions from algae? Ecol. Indic. 102, 599–607.
Yang, L., Hur, J., 2014. Critical evaluation of spectroscopic indices for organic matter source tracing via end member mixing analysis based on two contrasting sources. Water Res. 59, 80–89.
Yang, R., Wu, D., Li, Z., Yuan, Z., Niu, L., Zhang, H., Chen, J., Zhou, A., 2022. Holocene-Anthropocene transition in northwestern Yunnan revealed by records of soil erosion and trace metal pollution from the sediments of Lake Jian, southwestern China. J. Paleolimnol. 68 (1), 91–102.
Yang, X., Zhou, Y., Yang, X., Zhang, Y., Spencer, R.G., Brookes, J.D., Jeppesen, E., Zhang, H., Zhou, Q., 2024. Optical measurements of dissolved organic matter as proxies for CODMn and BOD5 in plateau lakes. Environ. Sci. Ecotechnol. 19, 100326.
Zhou, Y., Guo, H., Lu, H., Mao, R., Zheng, H., Wang, J., 2015. Analytical methods and application of stable isotopes in dissolved organic carbon and inorganic carbon in groundwater. Rapid Commun. Mass Spectrom. 29 (19), 1827–1835.
Zhou, Y., Davidson, T.A., Yao, X., Zhang, Y., Jeppesen, E., de Souza, J.G., Wu, H., Shi, K., Qin, B., 2018. How autochthonous dissolved organic matter responds to eutrophication and climate warming: evidence from a cross-continental data analysis and experiments. Earth Sci. Rev. 185, 928–937.